J Mater Sci (2010) 45:1744–1759
DOI 10.1007/s10853-009-4148-6

Morphological and phase dependence of nanotitania materials generated under extreme pH conditions for large scale production of TiO_2 nanowires (basic) and nanosquares or nanrods (acidic)

Timothy J. Boyle · Timothy N. Lambert · Harry D. Pratt III · Ping Lu · James J. M. Griego · Nancy Bush · Carlos A. Chavez · Margaret Welk

Received: 9 December 2009 / Accepted: 18 December 2009 / Published online: 8 January 2010

Abstract The effect that the phase of the starting nano-seed titania (TiO_2), the pH of the solvent solution, and the processing methodology employed have on the properties of the resultant TiO_2 nanomaterials were explored. This led to the development of a new process to produce large-scale, phase pure, thin nanowires of TiO_2 at high pH and nanosquares at low pH. Anatase, rutile, and Degussa P25^{TM} TiO_2 nanoparticle starting materials (or nanoseeds) were processed in strongly basic (10 M KOH) and strongly acidic (conc. HX, where X = Cl, Br, I) solutions using solvothermal (SOLVO) and solution precipitation (SPPT) methodologies. Under basic SOLVO conditions, the nanoseeds were converted to $H_2Ti_2O_5{\cdot}H_2O$ nanowires. The SPPT basic conditions also produced the same phased nanowires for the rutile and anatase nanoseeds, while the Degussa nanomaterial yielded mixed phased [anatase:rutile (9:1)] nanowires. The SPPT method was found to produce substantially thinner nanowires in comparison to the SOLVO route, with comparable surface areas but the strong basic media led to etching of the glassware yielding $HK_3Ti_4O_4(SiO_4)_3{\cdot}4H_2O$ nanorods. Hybridization of these two processing routes led to the use of Nalgene^{TM} bottle as the reaction flask termed the hybrid (HYBR) route, yielding even thinner $H_2Ti_2O_5{\cdot}H_2O$ nanowires on a large-scale. Switching to a concentrated halide acid (HX, where X = Cl, Br, I) system, SOLVO, SPPT, and HYBR routes were investigated. The resultant TEM images revealed that the rutile starting material yielded short rods, whereas the anatase seeds formed square or faceted materials.

T. J. Boyle (✉) · H. D. Pratt III · J. J. M. Griego · N. Bush
Advanced Materials Laboratory, Sandia National Laboratories, 1001 University Boulevard SE, Albuquerque, NM 87106, USA
e-mail: tjboyle@Sandia.gov

T. N. Lambert · C. A. Chavez
Department of Materials, Devices and Energy Technologies, Sandia National Laboratories, P.O. Box 5800, Albuquerque, NM 87185-0734, USA

P. Lu
Department of Materials Characterization, Sandia National Laboratories, P.O. Box 5800, Albuquerque, NM 87185-1411, USA

M. Welk
Department of Fuels and Energy Transitions, Sandia National Laboratories, P.O. Box 5800, Albuquerque, NM 87185-0734, USA

Introduction

Controlling the morphology of TiO_2 nanomaterials is a highly active area of research. In particular, there is an emphasis on the development of nano-wires, nano-rods, and nano-tubes [1–28] for use in such varied applications [1–40] as photovoltaics, bioceramics, sensors, catalysis, and lithium ion batteries. The majority of these TiO_2 nanomaterials have been generated either from the processing of TiO_2 nanopowders [1–13, 23] or in situ decomposition of titanium alkoxide [$Ti(OR)_4$] [14–22] precursors in highly concentrated aqueous basic solutions; however, acidic systems have been preliminarily explored, too [14, 18, 20–22, 24–28]. One of the fundamental concepts in the development of these controlled shaped nanomaterials is that select growth planes can be promoted or poisoned by changing the surface chemistry of the growth nuclei [23], which leads to asymmetric growth. This change is often easily accomplished by altering the pH of the growth media, which led us to investigate the morphological variations of nano-TiO_2 at extreme pH conditions.

Our interest in these systems stems from the need for a simple, high yield, large-scale procedure that produces morphologically varied nanoscale TiO_2 that will be used as fillers in nanocomposite materials. Nanofillers have been shown to improve the properties of the original matrix that are not achievable with larger particles [41–44], However, it has also been demonstrated that simply mixing nano-scaled particles into a matrix does not automatically result in the enhanced properties, since the nanofillers are not necessarily distributed in an isotropic manner [41–44]. Morphologically varied nanoparticles are being explored as a means to minimize this problem. Therefore, the first critical step is to generate controlled nanoparticles on a larger scale than is currently available.

This report details the synthesis of TiO_2 nanomaterials from commercially available TiO_2 nanopowders (anatase, rutile, and Degussa P25^{TM}-termed Degussa) at extreme pH conditions: high (10 M KOH) and low (conc. HX where X = Cl, Br, I) and our efforts to produce these on a larger scale than currently available. As the growth mechanisms are thought to originate off the nanoparticles [1–28], these starting TiO_2 nanopowders are, therefore, referred to as "nanoseeds." For the initial investigation, an established KOH solvothermal (SOLVO) methodology to TiO_2 nanowires was initially extended to a solution precipitation (SPPT) route and ultimately to a hybrid (HYBR) process that allows for the necessary large-scale synthesis. Relatively unexplored concentrated halide acid (HX, where X = Cl, Br, I) routes were also investigated to determine the different morphologies available for these low pH solution processes. This reports details the resultant morphologies observed for the phase, solution media, and processing routes employed.

Experimental section

The following chemicals were obtained from Aldrich and used without purification unless otherwise noted: TiO_2 nanomaterials (anatase, rutile, and Degussa), KOH, (conc.) HX (X = Cl (37%), I (55%)). HBr (48%) was obtained from Fluka.

Nanoparticle synthesis

Three routes were used to generate the TiO_2 nanomaterials of interest: (i) SOLVO, (ii) SPPT, and (iii) HYBR. The general route for each is outlined below for the basic and acidic route. All water (H_2O) used was deionized.

Basic

(i) *SOLVO*. The desired nanoseed precursor (0.200 g, 2.50 mmol) was added to a 10 M (aq.) KOH solution (30 mL) and sealed in a Teflon^{TM} lined Parr digestion bomb. The reaction was heated to 185 °C for 7 days. After this time, the bomb was allowed to cool to room temperature. The powder was separated from the mother liquor by centrifugation and washed thrice with water. The final powder was re-dispersed in water and the pH adjusted by (aq.) HCl (30%) until neutralized. The powder was then collected by centrifugation, washed with water (to remove KCl), and dried thoroughly to obtain dried TiO_2 powder. Starting materials (Yields g, %, color): Degussa (0.107 g, 54%, white), anatase (0.179 g, 90%, white), rutile (0.148 g, 74%, white). (ii) *SPPT*. TiO_2 (3.00 g, 37.5 mmol) was added to a stirring solution of 10 M (aq.) KOH (400 mL) in a glass round bottom flask. After heating at reflux for 3 days, the reaction was allowed to cool to room temperature and the resulting powder isolated as discussed above for the SOLVO route. Yields (g, %, color): Degussa (1.11 g, 37%, white), anatase (1.90 g, 63%, white), rutile (0.678 g, 23%, white). (iii) *HYBR*. A rutile TiO_2 sample (7.50 g, 9.38 mmol) was suspended in 10 M (aq.) KOH (~500 mL volume held constant) in a 1-L Nalgene^{TM} (polymethylpentene) bottle and heated for 3 days at 125 °C inside an oven with the cap loosely screwed onto prevent pressure build up. Additional water was added every 12 h to maintain the original volume level. After heating for 3 days, the reaction was allowed to cool to room temperature and the resulting powder isolated as discussed above for the SOLVO route. Yield (g, %, color): 4.94 g, 66%, white. Larger amounts were prepared by running several reactions side by side in the oven.

Acidic

(i) *SOLVO*. Rutile TiO_2 (0.200 g, 2.50 mmol) nanoseeds were added to 10 mL of DI H_2O in a Teflon^{TM} sleeve of a Parr^{TM} digestion bomb, followed by 10 mL of the desired conc. HX (X = Cl, Br, I). The reaction was sealed and then heated at 225 °C for 24 h. After this time, the reaction was allowed to cool to room temperature, the precipitate separated from the mother liquor by centrifugation, and washed thrice with DI water. The resulting powder was dried thoroughly in an oven at 130 °C. Yields (g, %, color): HCl (0.20 g, 100%, pale green), HBr (0.22 g, 110%, orange), and HI (0.25 g, 125%, pale brown). The more than theoretical yields noted here and below were attributed to the presence of residual H_2O. (ii) *SPPT*. Anatase TiO_2 (0.300 g, 3.75 mmol) was added to a stirring solution of 10 mL of conc. HX and 10 mL of water in a round bottom flask with a reflux condensor attached. After heating at reflux for 3 days under an argon atmosphere, the reaction was allowed to cool to room temperature and the resulting powder isolated as discussed above for the SOLVO route. Yields (g, %, color): HCl (0.426 g, 142%, off-white), HBr (0.258 g, 86%, white), and HI (0.338 g, 113%, yellow).

(iii) *HYBR*. A sample of rutile (0.200 g, 2.50 mmol) or anatase (0.200 g, 2.50 mmol) was suspended in a 1:1 mixture of HX:H_2O (~20 mL volume held constant) in a 250 mL Nalgene™ (polymethylpentene) bottle and heated for 1 day at 125 °C inside an oven with the cap loosely screwed onto prevent pressure build up. Water was added at 12 h to maintain the original volume level. After heating, the reaction was allowed to cool to room temperature and the resulting powder isolated as discussed above. Yields (g, %, color): anatase: HCl (0.191 g, 96%, beige), HBr (0.010 g, 5%, beige), and HI (0.005 g, 3%, white); rutile HCl (0.175 g, 88%, beige), HBr (0.144 g, 72%, beige), and HI (0.088 g, 44%, orange).

Characterization

Powder X-ray diffraction (PXRD)

Dried and washed powders were mounted directly onto a Si zero background holder purchased from the Gem Dugout. Phase identification for the nanoscale materials was determined PXRD patterns collected on a PANalytical powder diffractometer employing Cu Kα radiation (1.5406 Å) and a RTMS X'Celerator detector. Samples were scanned at a rate of 0.02°/2 s in the 2θ range of 10°–100°. Patterns were analyzed using the Jade Software Program [45].

Brunauer–Emmett–Teller (BET) surface area analysis

N_2 adsorption/desorption on ~100–200 mg of a sample was measured using a Micrometrics ASAP 2020 sorptometer.

Transmission electron microscopy (TEM)

An aliquot of the TiO_2 nanopowder dispersed in methanol was placed directly onto a holey carbon type-A, 300 mesh, copper TEM grid purchased from Ted Pella, Inc. The aliquot was then allowed to dry. The resultant particles were studied using one of two instruments: the Philips CM 30 TEM with the Thermo Noran System Six Energy Dispersive X-ray (EDX) System or the FEI Tecnai TF30 TEM/STEM with the EDAX EDX System, both operating at 300 kV accelerating voltage.

Scanning electron microscopy (SEM)

The samples were dispersed onto carbon tape and sputter coated with gold–palladium. Samples were imaged using a Zeiss Supra 55VP field emitter gun scanning electron microscope (FEGSEM). A Noran EDS detector and Noran System Six software was used for the acquisition of EDS spectra.

Discussion and results

The exploration of the large-scale production of complex nanomaterials grown from TiO_2 nanoseeds under extreme pH conditions was performed using 10 M (aq.) KOH (high) and concentrated (aq.) HX (low) as solvents. Tables 1 and 2 summarize the results. Initially the starting powders used were characterized by TEM and PXRD to establish a baseline of size, morphology, and purity. As can be observed in Fig. 1, the Degussa materials were random spherical nanomaterials 10–50 nm in size and composed of a mixture of ~9:1 anatase (JCPDS card No. 00-21-1272): rutile (JCPDS card No. 00-21-1276). In contrast, the Aldrich anatase or rutile nanomaterials were found to be phase pure dots (>10 nm) or whiskers, respectively, of varied nanometer dimensions. These TiO_2 nanoseeds were used without further modifications.

High pH

As mentioned, there are numerous routes for the production of TiO_2 nanowires using high pH solvent systems [1–23]; however, the majority of these routes involve hydrothermal syntheses in a Parr digestion bomb, which severely limits the amount of material that can be generated (typically ~200–500 mg for a 50 mL scaled reaction). We became interested in the route reported by Tian et al. [12, 13] to produce high aspect ratio TiO_2-B nanowires from the treatment of nanotitania (Degussa—a mixture of anatase and rutile, see Fig. 1a) with 10 M KOH in a Parr digestion bomb for 7 days.

SOLVO synthesis

Initial efforts focused on reproducing the SOLVO route [12, 13]. As the DeGussa starting material was mixed phase, determining the role that the starting TiO_2 nanoseed phase had on the final nanowire phase became a critical issue. Dugussa TiO_2 nanomaterials were suspended in 10 M KOH and heated for 7 days in a Parr Digestion bomb. The resultant TiO_2 nanowires isolated were initially indexed to TiO_2-B phase [46] (JCPDS card No.: 00-046-1238); however, further analysis indicated a slightly better fit was obtained for $H_2Ti_2O_5{\cdot}H_2O$ (JCPDS card No.:00-47-0124). Previous work by Sugita et al. indicates that the hydroxide phase can be formed as a product of hydrothermal synthesis [47]; whereas, Tian et al. report their initial materials adopted a titanate phase (JCPDS card No.: 47-0561), which was after high temperature treatment converted to the TiO_2-B phase [46] (JCPDS card No.: 00-046-1238). Based on these results, the nanowires were tentatively identified as $H_2Ti_2O_5{\cdot}H_2O$, but further work is necessary to fully identify this phase.

Table 1 Comparison of the TiO_2 nanomaterial generated by 10 M KOH following SOLVO, SPPT, and HYBR routes

	Degussa	Anatase	Rutile
Starting material			
Phase	90% anatase 10% rutile	100% anatase	100% rutile
Morphology	Dots	Dots	Whiskers
Surface area (m^2/g)	46	128	202
SOLVO			
Final phase	$H_2Ti_2O_5 \cdot H_2O$	$H_2Ti_2O_5 \cdot H_2O$	$H_2Ti_2O_5 \cdot H_2O$
Morphology	Wires/particles	Wires	Wires
Aspect ratio	44 wires Particles (37 nm)	27	53
Surface area (m^2/g)	146	394	497
SPPT			
Final phase	Anatase/rutile	$H_2Ti_2O_5 \cdot H_2O$	$H_2Ti_2O_5 \cdot H_2O$
Morphology	Wires/particles	Wires	Wires
Aspect ratio	54 wires Particles (45 nm)	47	82
Surface area (m^2/g)	164	354	361
HYBR			
Final phase	–	–	$H_2Ti_2O_5 \cdot H_2O$
Morphology	–	–	Wires
Aspect ratio	–	–	95
Surface area (m^2/g)	–	–	72

–, Data not obtained

Table 2 Comparison of the TiO_2 nanomaterial generated by HX following SOLVO, SPPT, and HYBR routes

ACID	HCl		HBr		HI	
SOLVO						
Final phase	Anatase	Rutile	Anatase	Rutile	Anatase	Rutile
Morphology	Square	Rod	Square	Rod	Square	Rod
Aspect ratio	–	5	–	3	–	3
Surface area (m^2/g)	–	58	–	101	–	94
SPPT						
Final phase	Anatase	Rutile	Anatase	Rutile	Anatase	Rutile
Morphology	Particles	Particles	Particles	Particles	Particles	Particles
Surface area (m^2/g)	136	–	127	–	131	–
HYBR						
Final phase	Anatase	Rutile	Anatase	Rutile	Anatase	Rutile
Morphology	Particles	Rods	Particles	Rods	Particles	Rods
Aspect ratio	–	5	–	5	–	5
Surface area (m^2/g)	119	197	233	212	–	222

–, Data not obtained

Figure 2 shows the TEM images obtained for these materials. As can be observed, the nanowires had a similar diameter as the starting nanoseed with an aspect ratio approaching 10. Further studies using the Aldrich anatase (10–25 nm dots in diameter, Fig. 1b) or rutile (10–25 nm diameter whiskers, Fig. 1c) nano-TiO_2 materials under identical conditions, yielded similar phased nanowires as determined by powder X-ray diffraction (PXRD) and TEM analyses (see Fig. 2b–c). The Degussa nanowires had a PXRD pattern that was much sharper

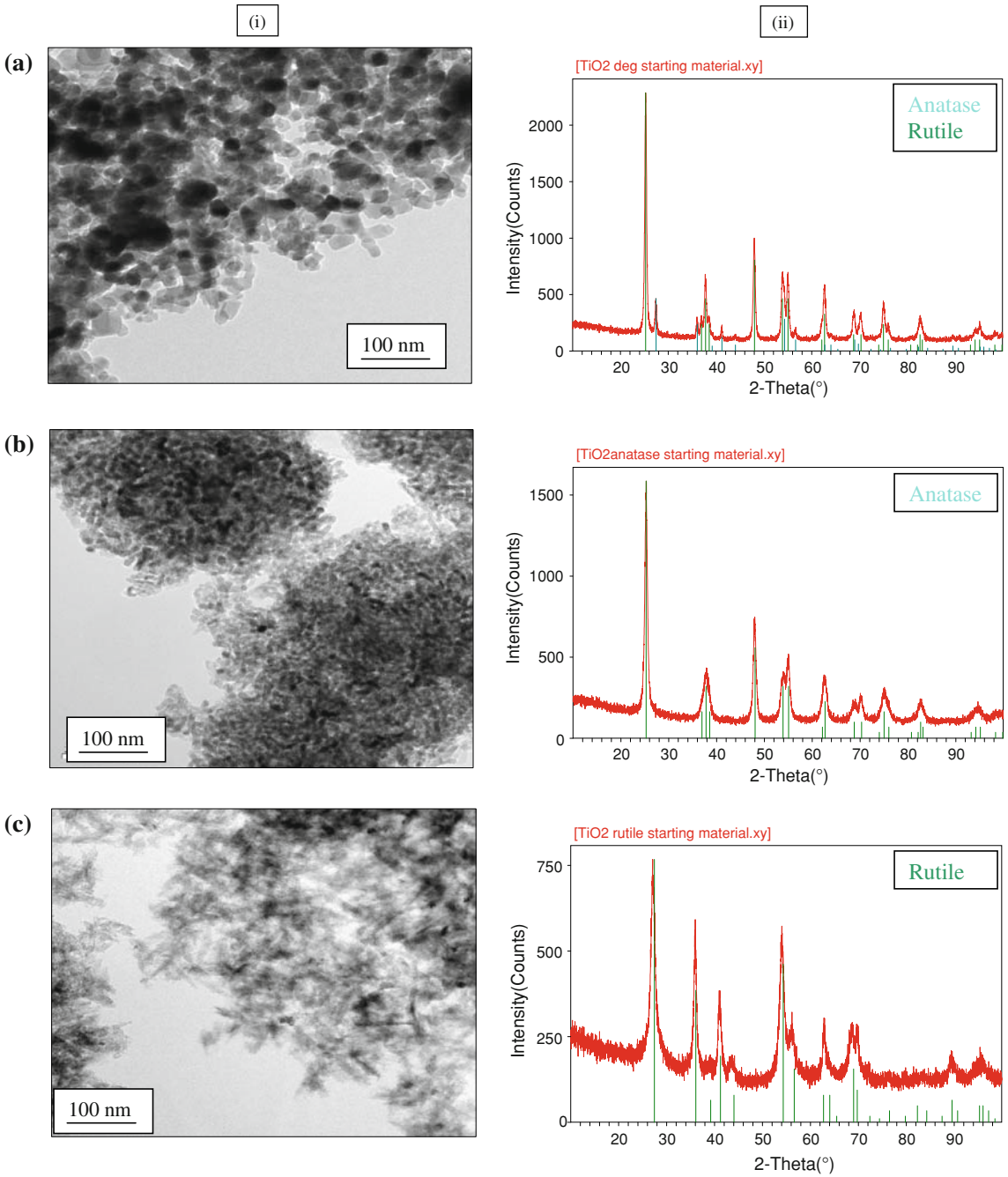

Fig. 1 (i) TEM and (ii) PXRD patterns of starting materials **a** Degussa, **b** anatase, **c** rutile

than the other two samples. Again, the diameter of the nanowire was essentially the same as the starting nanoparticle. BET adsorption analyses (Table 1) gave surface areas of 46, 128, and 202 m^2/g for the starting nanoseeds from the Degussa, anatase, and rutile, respectively, which generated nanowires with 146, 394, and 497 m^2/g surface areas. There is a significant increase in the final surface areas present after growing the wires. Furthermore, rutile nanoseeds appear to generate the highest surface area nanowires under the conditions employed.

A temporal study of the morphological changes that occurred in this reaction was undertaken over a 7-day period at 24 h intervals from seven identical reaction setups. TEM images indicate that nanowires formed within 24 h with no further morphological changes noted. Upon further heating, the nanowires were found to remain amorphous until >3 days had elapsed. Upon crystallization, the thermodynamically favored nanowires formed independent of the phase of the starting material.

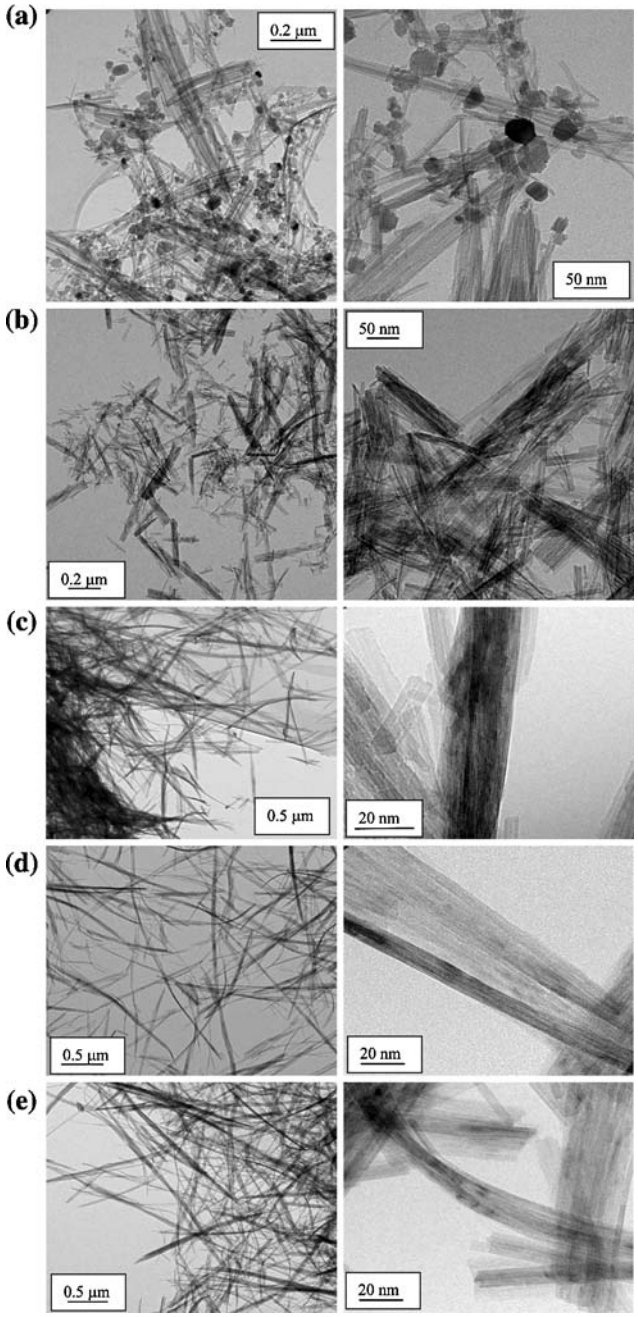

Fig. 2 TEM of TiO_2 materials from 10 M KOH (aq.) processing by SOLVO route **a** Degussa, **b** anatase, **c** rutile (day 1), **d** rutile (day 3), **e** rutile (day 7)

SPPT synthesis

Nanowires were rapidly formed from the SOLVO routes and this led to the possibility of using solution precipitation (SPPT) route. SPPT routes were of interest since large amounts (50–100 g) of the nanorods required for subsequent nanocomposites studies could be generated under batch-like processing methodologies. One report of a solution precipitation (SPPT) route for the production of TiO_2 nanowires is available, where Daoud and Pang report on the formation of anatase and TiO_2-B nanowires from TiO_2 nanotubes (prepared from anatase nanopowders in 10 M KOH) heated in a 10 M KOH solution at a variety of temperatures and times [46].

A similar synthesis as described above was undertaken replacing the TiO_2 nanotubes by the Degussa, anatase, or rutile nanoseeds. A temporal SPPT study was undertaken through aliquot analyses monitoring using TEM and PXRD (see Fig. 2c–e). While wires were formed for all precursors, the TEM images clearly indicate that more than 24 h was necessary to generate the desired high aspect ratio wires. The final conditions used, described in "Experimental section" were optimized and consisted of heating a suspension of the TiO_2 nanoparticles at reflux temperature for 3 days in 10 M KOH under an argon atmosphere.

Figure 3 shows the SEM and PXRD of the final products isolated at the end of the reaction following workup as described in "Experimental section". As can be discerned from the SEM images, all precursors generate nanowires with an aspect ratio of greater than 200 that were significantly thinner than those noted for the SOLVO route. BET adsorption analysis gave surface areas of 164, 354, and 361 m^2/g for the final nanowires formed from Degussa, anatase, and rutile, respectively. While the nanowires show slightly decreased surface areas in comparison to the SOLVO route, these data suggest that the SPPT route was an acceptable alternative and could be used for larger scale preparation of nanowires. Interestingly, the Degussa nanoparticles retained the original ~9:1 (anatase:rutile) mixed phase (Figs. 1a and 3a), while the anatase and rutile powders were converted to the $H_2Ti_2O_5{\cdot}H_2O$ phase. For the DeGussa generated nanomaterials, residual KCl was noted as well. Again, it appears that the Degussa material is much more crystalline than either the anatase or rutile nanowires. At this time, we are uncertain as to why the Degussa generated nanomaterials are so differentiated from the pure starting materials and studies are underway to explore this phenomenon. Due to its phase purity and consistently high surface areas materials generated, the commercially available rutile (Aldrich) precursor was the preferred nanoseed material.

From the onset, the possibility of contamination or incorporation of silicon oxide from the reaction of the strong KOH base solution with the glassware in the SPPT setup was of concern. While our initial results did not reveal detectable Si levels in the EDX analysis, recovery, and reuse of the KOH solutions in the same glassware rapidly (<3 preparations) led to significant etching of the round bottom flask. Eventually, contamination of the nanowires with Si occurred at such a level that the titanium silicate phase [$HK_3Ti_4O_4(SiO_4)_3{\cdot}4H_2O$; JCPDS card No.: 00-047-0043] formed (Fig. 4). SEM analysis revealed that

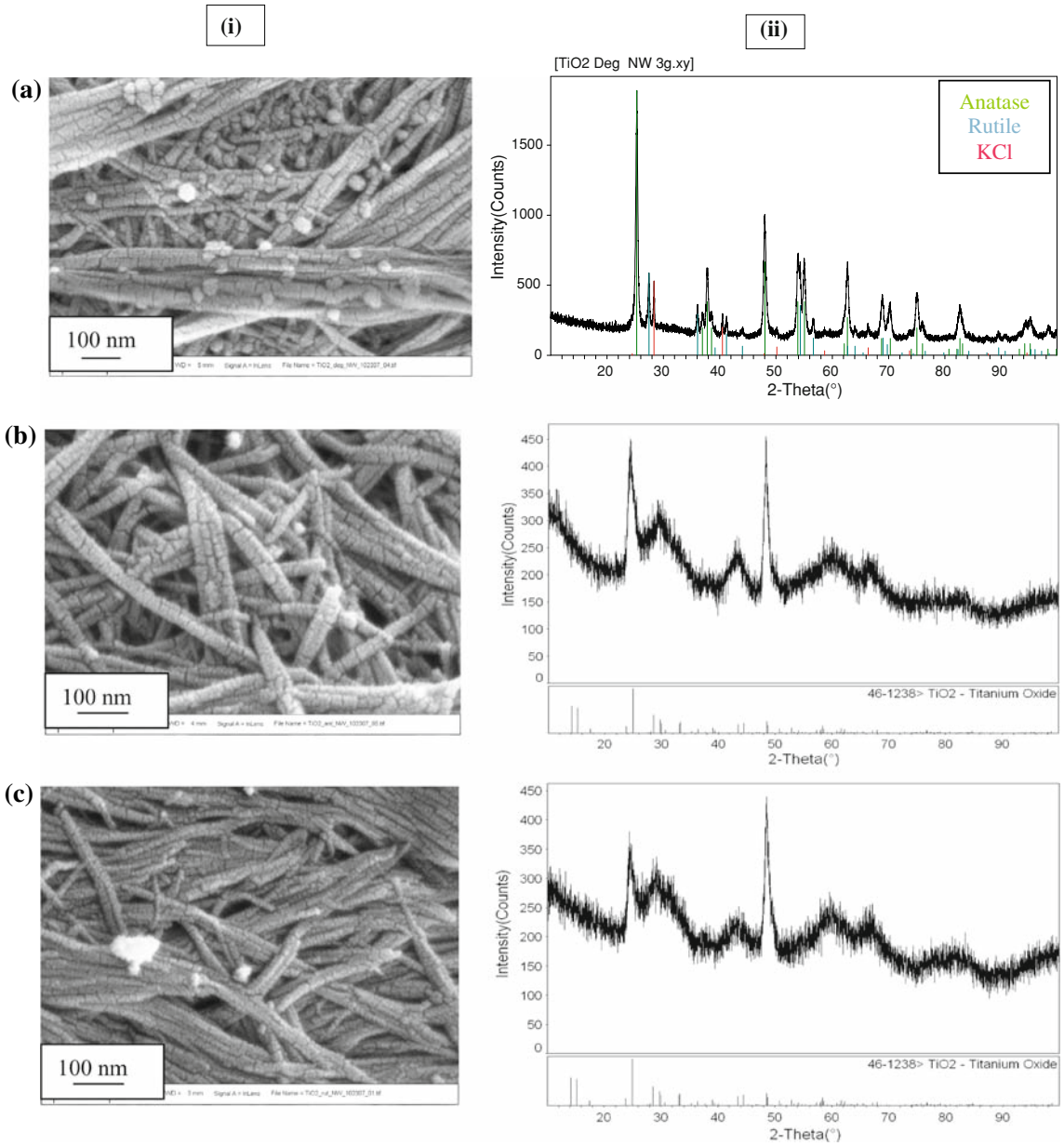

Fig. 3 (i) TEM and (ii) PXRD patterns images of nanowires generated by 10 M KOH (aq.) SPPT route **a** Degussa, **b** anatase, **c** rutile. Reticulation is from Au/Pd sputter coat for SEM

the primary morphology was still a nanowire with diameters of 20–40 nm and similar aspect ratios to that of the other nanowires. The potential for silicate contamination in the nanowires, even for the first attempts is, therefore, highly likely. However, these results also indicate that the rationally controlled synthesis of titanium silicate nanowires can be achieved when desired [48–50].

HYBR

As SOLVO and SPPT routes proved problematic in terms of generating phase pure TiO_2 on large scale, an additional alternative method was needed. A hybrid-processing route combining the SOLVO and SPPT routes was, therefore, developed focusing on rutile starting materials, as they consistently generated the highest surface area nanomaterials. The HYBR route consisted of using Nalgnene™ bottles that were partially filled with the TiO_2/KOH reaction mixture, loosely capped to minimize solvent loss, and re-filled periodically with water to ensure a constant reaction volume. The reaction was heated for 3 days at 125 °C in an oven and the subsequent product was also found to be nanowires (shown in Fig. 5). The wires formed have an aspect ratio approaching 95 with the width of the wires

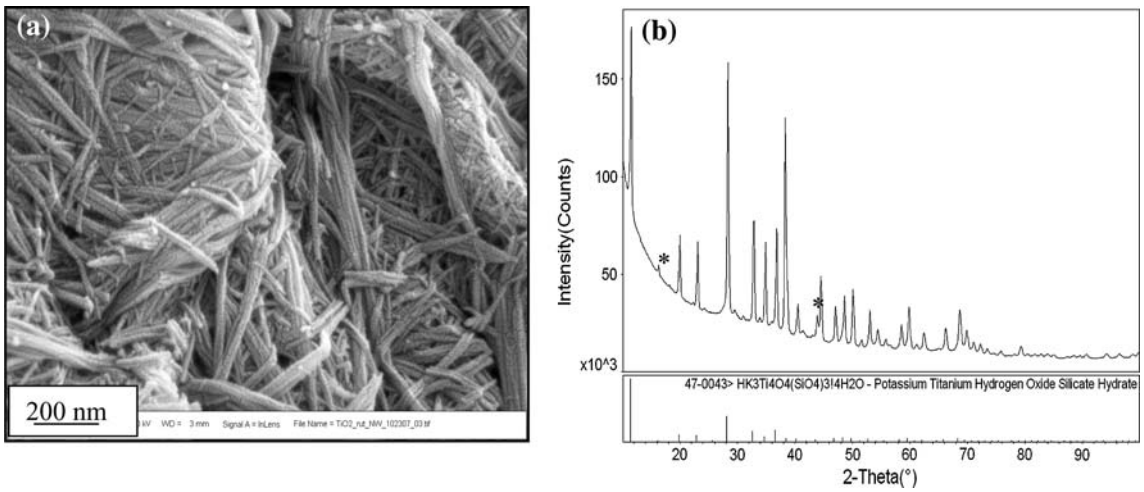

Fig. 4 $HK_3Ti_4O_4(SiO_4)_3{\cdot}4H_2O$ nanowires: **a** SEM and **b** PXRD pattern (* indicates substrate)

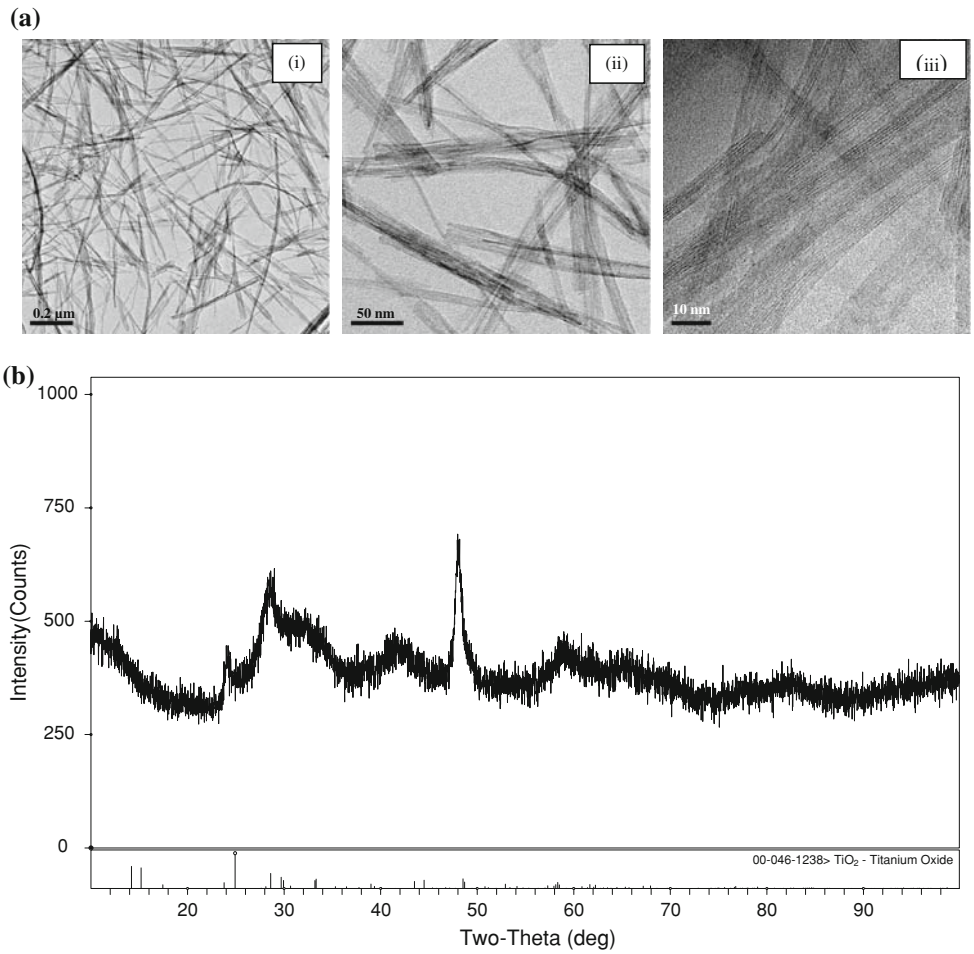

Fig. 5 TiO_2 materials generated from 10 M KOH (aq.) HYBR routes using rutile starting nanomaterial: **a** TEM images with scale bars of: (i) 0.2 µm, (ii) 50 nm, and (iii) 10 nm and **b** PXRD pattern

significantly thinner than those nanowires observed in the SPPT (or SOLVO) routes. Additionally, these nanowires appear to be less "bundled" than the other routes but have a lower aspect ratio. BET data show the nanowires to have a significantly smaller surface area of 72 m^2/g, than those formed via the SOLVO or SPPT routes. Large-scale syntheses of these nanomaterials were readily achieved by running multiple reactions at the same time. Table 1 summarizes the variables noted for the different optimized process to nanowires using 10 M KOH.

Low pH

While it appears the hybrid basic route was a useful large-scale route for the production of nanowires, several reports have indicated that acid routes may also be viable method for the production of other more complex TiO_2 nanomorphologies [14, 18, 20–22, 24–28]. By lowering the pH, the functional groups on the surface growth planes will be altered and thus different growth planes will be favored yielding alternative morphologies. Typically, the reported acidic possessing involves the reaction of $Ti(OR)_4$ added into simple acids such as acetic acid [21], nitric acid, and trace amounts of HCl followed by aging and then hydrothermal processing. Recently, it was reported that HF could also play a role in determining the shape of the final nano TiO_2 [24–27]. In this reaction F-doped TiO_2 flowerlike nanomaterials were synthesized by the acidification of Ti^0 plates in HF under solvothermal (SOLVO) conditions [27]. Additionally, the use of the congener halide acids (HX) in the production of TiO_2 nanoarrays have only been investigated in a limited manner but have the potential for production of morphologically varied nanomaterials [18, 28, 51–53]. For example, parallelepiped shaped nanoparticles ranging from 7 to 100 nm in size were prepared hydrothermally using $Ti(OCHMe_2)_4$ modified with catalytic amounts of HCl [14, 18]. With the fact that the HXs would impart some effect over TiO_2 nanomaterial morphology [18, 51–53], it was of interest to determine what morphologies SOLVO, SPPT, and HYBR synthetic routes using (conc.) HX (where X = Cl, Br, I) solutions and TiO_2 nanomaterials would produce, especially since TiO_2 is widely reported to not be soluble in HX solutions.

Rutile or anatase nanoseeds were placed into HX at different molarities. Degussa starting materials were avoided due to the mixed phases, which could add another variable that would complicate the final interpretation. HF was avoided due to the safety concerns. The various results obtained for these nanoseeds under the different acids and processing routes are tabulated in Table 2. The three routes used previously were investigated using the phase pure TiO_2 (anatase and rutile) at low pH.

SOLVO synthesis

The SOLVO TiO_2 nanoseeds growth investigation at low pH was undertaken in a similar manner as noted for the high pH solutions. To a slurry of seeds in H_2O, and equal volume of conc. HX was added and the mixture sealed in a Teflon™ lined Parr digestion bomb. There was no indication of a reaction occurring upon mixing. After heating at 225 °C for 24 h, the reaction mixture was removed and allowed to cool. The resulting precipitate isolated by centrifugation, was washed repeatedly with H_2O, and then an aliquot was deposited onto the TEM grid. The anatase results are shown in Fig. 6 (TEM i: a–c, PXRD ii: a–c) and rutile in Fig. 7 (TEM i: a–c, PXRD ii: a–c). For both precursors, substantially different morphologies were isolated in comparison to their parent nanoseeds (Fig. 1). Independent of the acid employed (Figs. 6(i: a–c) and 7(i: a–c), both the anatase and rutile starting seeds maintained their respective phase as can be determined from the PXRD patterns (Figs. 6(ii) and 7(ii)); JCPDS Nos.: 00-21-1272 anatase and 00-21-1276 rutile, respectively).

For anatase staring materials, the products isolated were all similar in shape, forming squares (see Fig. 6) for each acid reaction. EDX does not reveal the presence of any halide incorporation, which further confirms the >100% yields obtained was in fact due to water retention. The squares have very well-defined edges with rounded corners. Most of the squares are ~30 nm in size with a noticeable amount of smaller squares. For the HCl product (Fig. 6a), the squares are varied in size ranging from 15 to 50 nm with fairly regular edges. In contrast, the HBr products (Fig. 6b) present slightly larger less-defined edges. The most regular squares were isolated for the strongest acid HI (Fig. 6c) and may reflect a slightly higher degree of solubility versus the other weaker acids.

In contrast, rods were isolated for the rutile whisker starting material, again independent of the acid employed. In this instance, the HBr generated rods are smaller and more polydispersed in aspect ratio than either of the other acids. The HCl (weakest) and HI (strongest) acids have similar uniform nanorods of ~20 nm width with a range of lengths (50–90 nm) but no rod appears to be longer than 100 nm in length. Lower processing temperatures (175 °C) also led to similar dimensioned rods. BET analyses of the rutile materials indicated that the HCl (58 m^2/g) nanorods had less surface area than either the HBr (101 m^2/g) or HI (94 m^2/g) nanorods.

Interestingly both of the precursors in HX do *not* form wires as noted for all of the KOH systems. The variations between the two nanomaterials' morphology is either a reflection of the starting structure or the "solubility" of the TiO_2 phase in acid which will alter its surface chemistry. While both anatase ($I4_1/mmm$, $a = b = 3.78$ Å, $c = 9.51$ Å, $V = 136.25$ $Å^3$, $Z = 4$), and rutile ($P4_2/mmm$, $a = b = 4.58$ Å, $c = 2.95$ Å, $V = 62.07$ $Å^3$, $Z = 2$) crystallize in the $4/mmm$ tetragonal crystal system, rutile has the lower molecular volume with a unit cell atom arrangement that is more symmetric in comparison to the more open elongated anatase structure [54]. Therefore, to generate a square- or rod-like morphology would require asymmetrical growth and preferred orientation for either phase. There is little to poison the faces of the growth particles based on the three component system (HX,

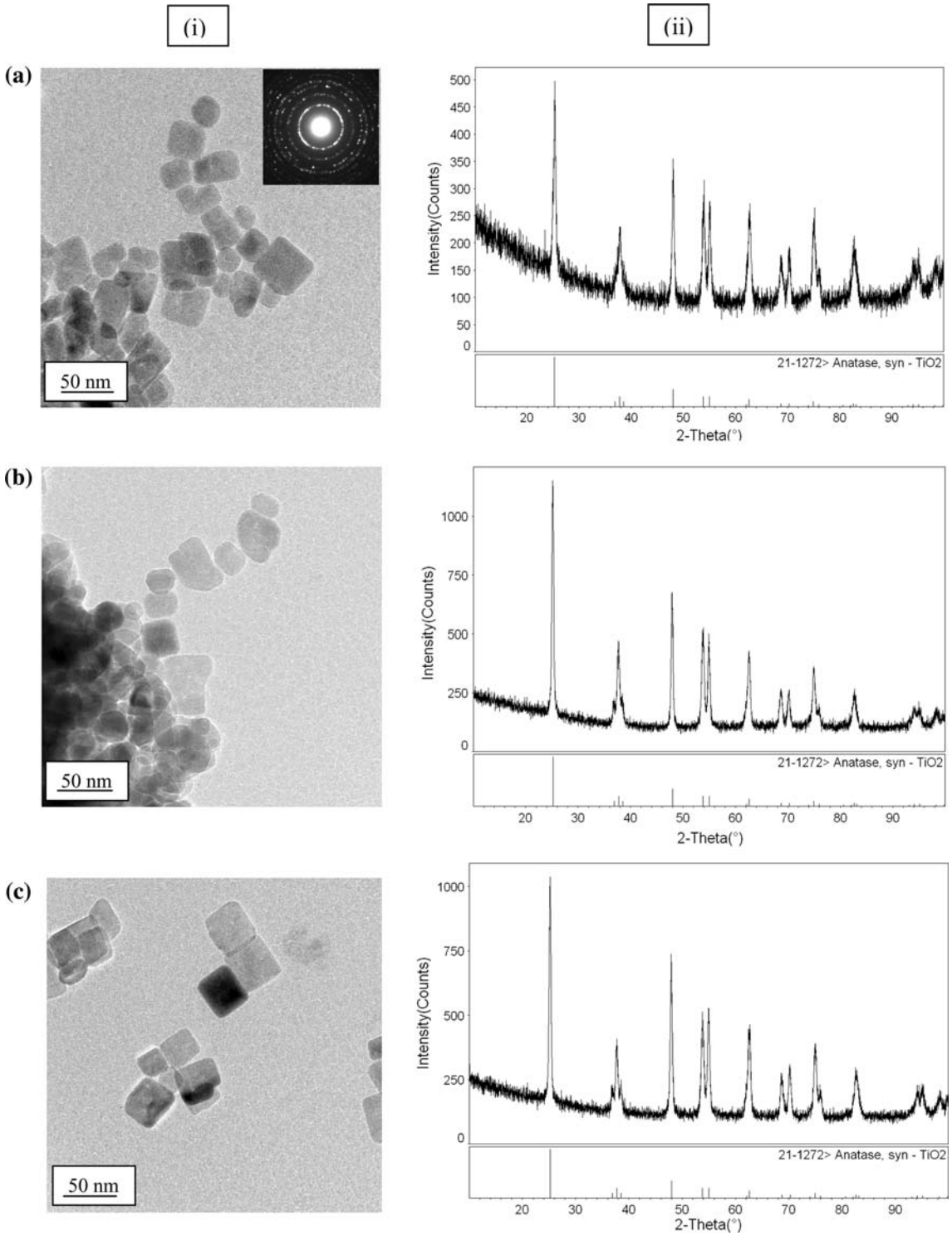

Fig. 6 Anatase: (i) TEM images and (ii) PXRD patterns of TiO_2 from SOLVO route using 1:1 H_2O and HX (conc.): **a** HCl (*inset* SAED pattern), **b** HBr, **c** HI

H_2O, and TiO_2). Therefore, the degree of protonation of the structure likely accounts for the directed growth observed. It has been shown that the (001) surface of anatase is not as reactive as the (101) facets [55] and that the (110) of rutile is more reactive than the (001) surface [56]; therefore, these are proposed to be the favored growth planes.

To confirm this, a series of high-resolution TEM analyses were undertaken and the resultant information

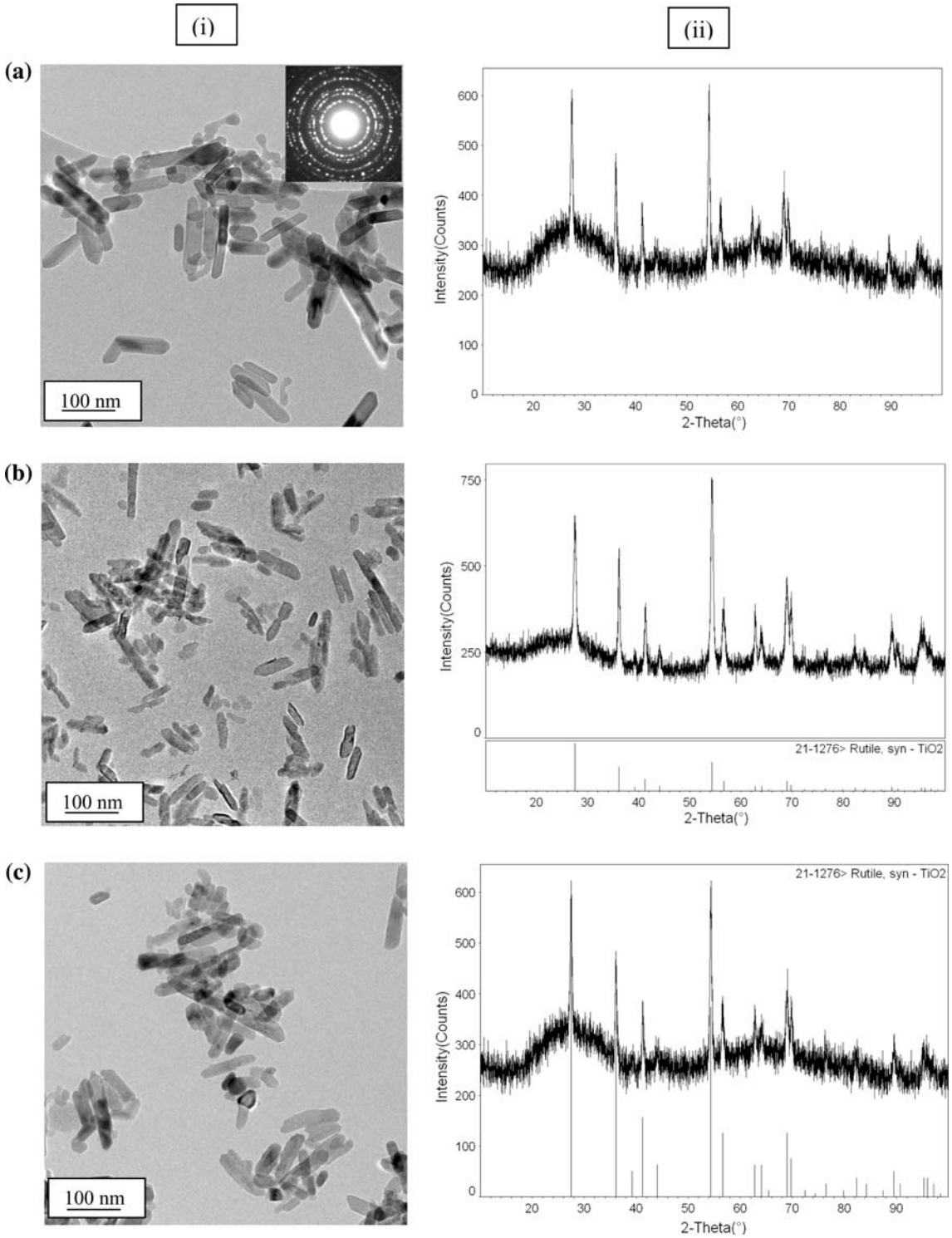

Fig. 7 Rutile: (i) TEM images and (ii) PXRD patterns of TiO_2 from SOLVO route using 1:1 H_2O and HX (conc.): **a** HCl (*inset* SAED pattern), **b** HBr, **c** HI

pertaining to the squares is shown in Fig. 8 and the rods in Fig. 9. Selected area electron diffraction confirms that the squares adopt the anatase phase and the rods have a rutile structure—in agreement with the PXRD data (vide infra). Tilting experiments indicate that the squares are relatively thin with the ratio of the plate thickness to the width of the edge approaching 0.5. While there is a disparity in the shape and size of the particles, the square species have the larger plate growing along the (001) or *c*-axis and the edges associated with the (100) axis. The (101) lattice spacing

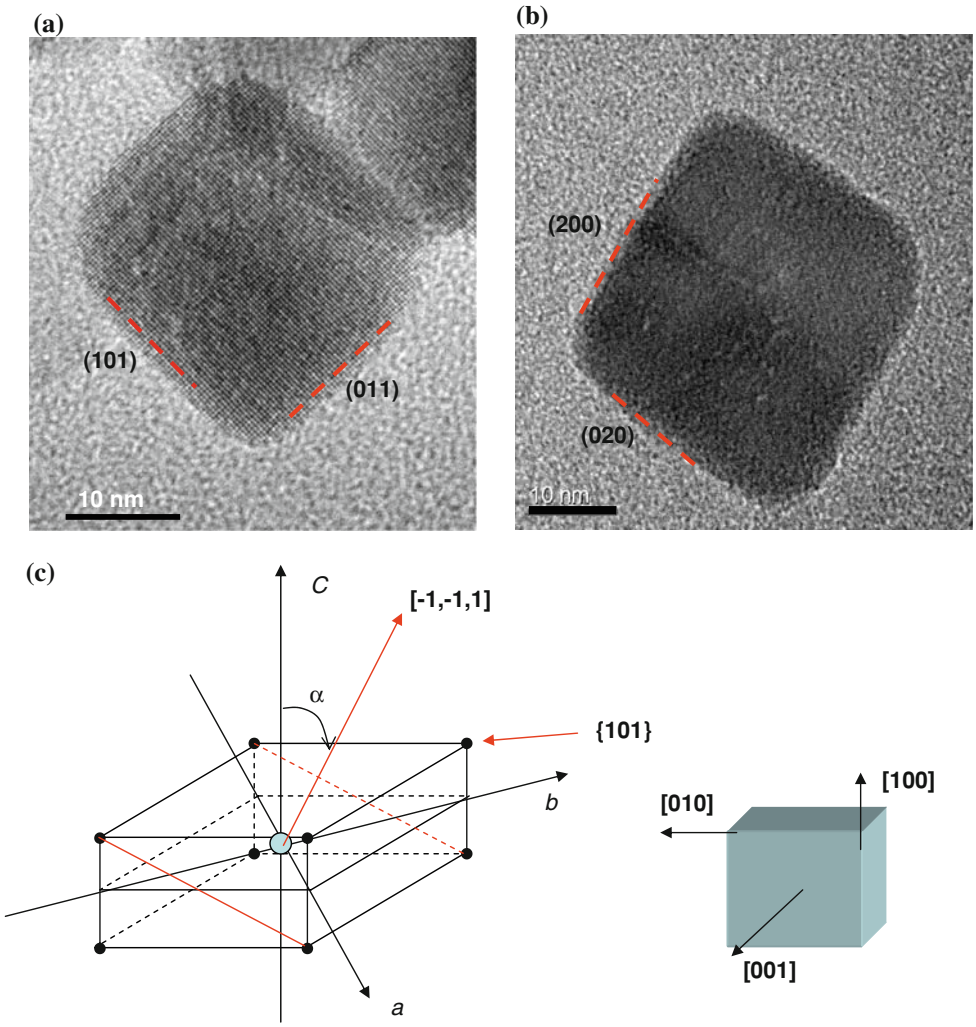

Fig. 8 HRTEM image taken in **a** [−1, −1, 1] and **b** (001) direction of TiO_2 squares generate by the SOLVO route, **c** schematic of cell

was clearly shown to be 0.352 nm, whereas the (200) spacing of 0.189 nm was much harder to record. The growth along the *c*-axis is unexpected due to its reported lower reactivity [55]. HRTEM images indicate that the rod is growing along its (001) or the *c*-axis, again in contrast to the expected growth planes [56]. The edges of the rods are the (110) planes with the tip of the rod bounded by four faceted (111) planes.

SPPT synthesis

While the square morphologies observed above for the low pH SOLVO route were of potential interest for composite fillers, as previously discussed this methodology is not amenable to large-scale processing. Therefore, we investigated nanomaterials generated from the SPPT route at low pH. Concerns about etching of the glass to form silicates were not warranted for the HX (HX = Cl, Br, I) reactions. The similarities of the final TiO_2 morphology noted for the SPPT and SOLVO routes at high pH implied the low pH route morphologies might also be comparable.

For the SPPT processing, the anatase TiO_2 powder (Fig. 1c) was the first seed investigated. It was placed in a three neck round bottom with water, an equal volume of HX was added, and then the reaction mixture was heated to reflux under an argon atmosphere for 3 days. After this time, the precipitate was isolated by centrifugation, washed with water, and then analyzed by TEM and PXRD (see Fig. 10). BET analyses of the anatase generated materials indicated that the HCl (136 m^2/g), HBr (127 m^2/g), and HI (131 m^2/g) all possessed approximately the same surface area. Rutile particles were also investigated with similar results. While larger particles were obtained for each starting material, the shapes were not regular and did not warrant further study; hence, further efforts concerning this route were not pursued.

HYBR route

Due to the lack of interesting morphologies noted for the SPPT method, the HYBR route was explored at low pH. This was undertaken since it is amenable to large-scale

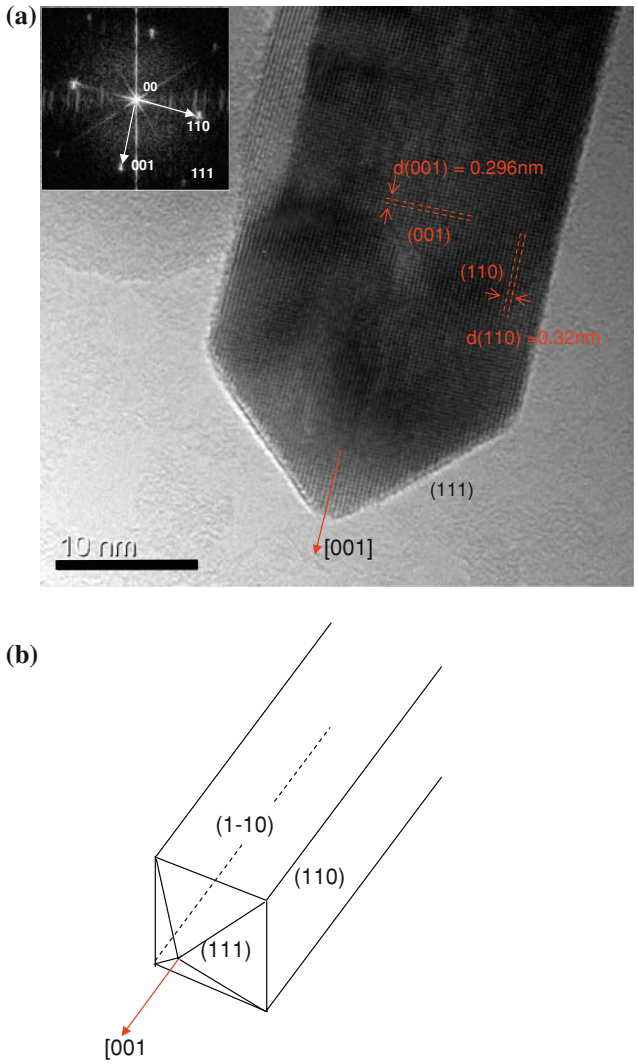

Fig. 9 **a** HRTEM micrograph taken in [1, −1, 0] electron beam direction of nanorods from SOLVO, **b** schematic of cell: rod is growing along its [001] or *c*-axis and has four {110} planes on the sides, the tip of rod is bounded by four faceted {111} planes

synthesis and the nanoparticle morphologies observed for the high pH SOLVO and HYBR routes were similar. TEM analyses of the low pH HYBR route indicated that some morphological variations were noted for both starting materials and acids investigated. For anatase, the TEM images (Fig. 11a) displayed square-like morphologies but the edges were not as defined for these materials as noted for the SOLVO route. However, the anatase phase was noted for the HCl and HBr solvent systems, whereas the HI had an amorphous material (Fig. 11b). In contrast, the rutile (Fig. 12) phase formed thin wires that agglomerated. Again, the rods formed in the SOLVO route were larger and more defined in comparison to the HYBR method. The PXRD patterns indicated that the rutile phase was retained upon conversion (Fig. 12b). The BET analyses of the anatase and rutile materials generated by the HYBR route

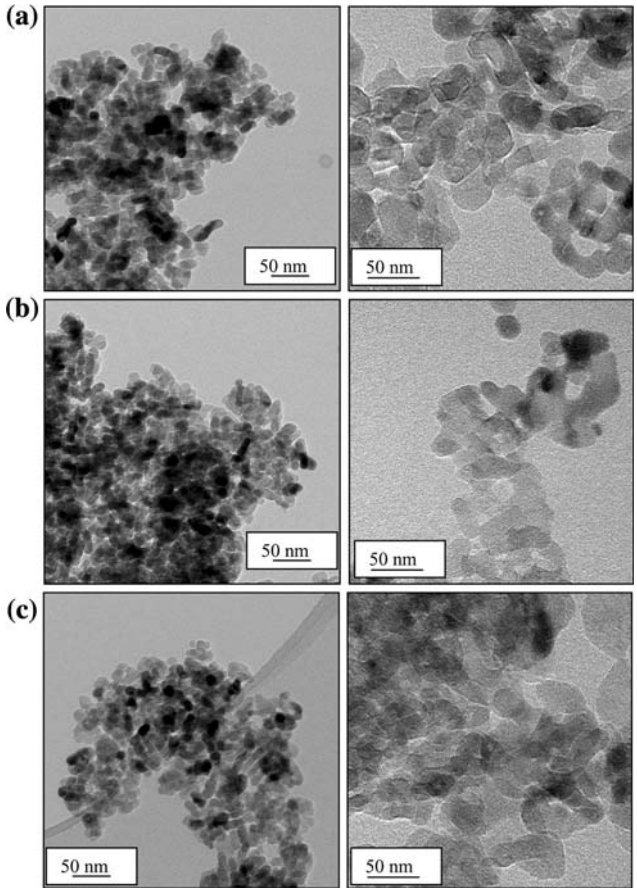

Fig. 10 TEM images of TiO_2 from SPPT route **a** HCl, **b** HBr, **c** HI

found that the HCl-derived material had less surface area than either the HBr or HI. Longer reaction times are being explored for the HYBR route to improve the morphology but retention of the reaction volume is difficult due to evaporation of both water and the acid. The surface areas of the materials generated by the HYBR route appear to be the largest of the HX solvent systems investigated (Table 2). Large-scale HYBR reactions were not attempted due to the constant monitoring required to maintain proper solution levels based on the higher volatility of the HX solutions in comparison to the KOH reactions. However, with a properly optimized/engineered setup, the HBYR route is amenable to large-scale processing to generate the interesting square-like morphologies.

Summary and conclusions

The standard SOLVO and SPPT routes that employ TiO_2 nanomaterial precursors heated in 10 M (aq.) KOH were found to be inadequate for production of large-scale nanowires of TiO_2. The SOLVO routes are limited by size of the Parr digestion bomb that can be used and the SPPT route led to etching of the glassware and ultimately forming

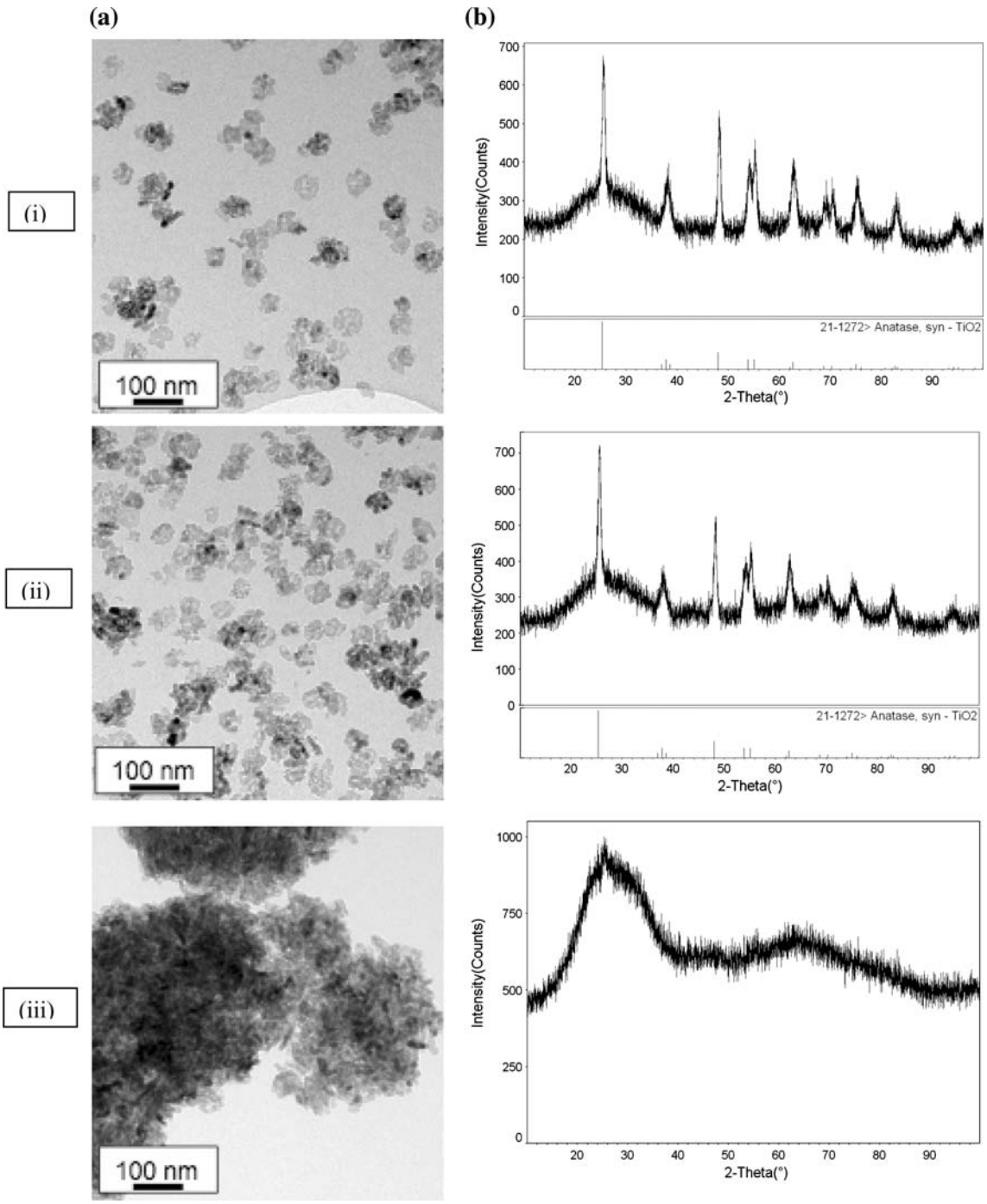

Fig. 11 TiO_2 materials generated from HX HYBR route using anatase starting nanomaterial: **a** TEM images with (100 nm) scale bars and **b** PXRD pattern of: (i) HCl, (ii) HBr, and (iii) HI

$HK_3Ti_4O_4(SiO_4)_3{\cdot}4H_2O$ nanowires. Therefore, a facile large-scale HYBR route that involves heating TiO_2 in 10 M KOH in a Nalgene™ bottle was successfully developed. Interestingly, Degussa starting nanoseeds maintained their 9:1 anatase:rutile composition from the SPPT route, whereas all other routes and precursors formed the $H_2Ti_2O_5{\cdot}H_2O$ phased nanowires. The surface area of the nanowires decreased according to the methods employed (SOLVO > SPPT > HYBR) with rutile nanoseeds yielding the highest surface areas for each method explored.

Switching to halide acids as the solvent, led to the retention of parent seed particles' phase for the final nanomaterials, independent of the solvent acid or process employed. The SPPT and HYBR routes led to less-defined

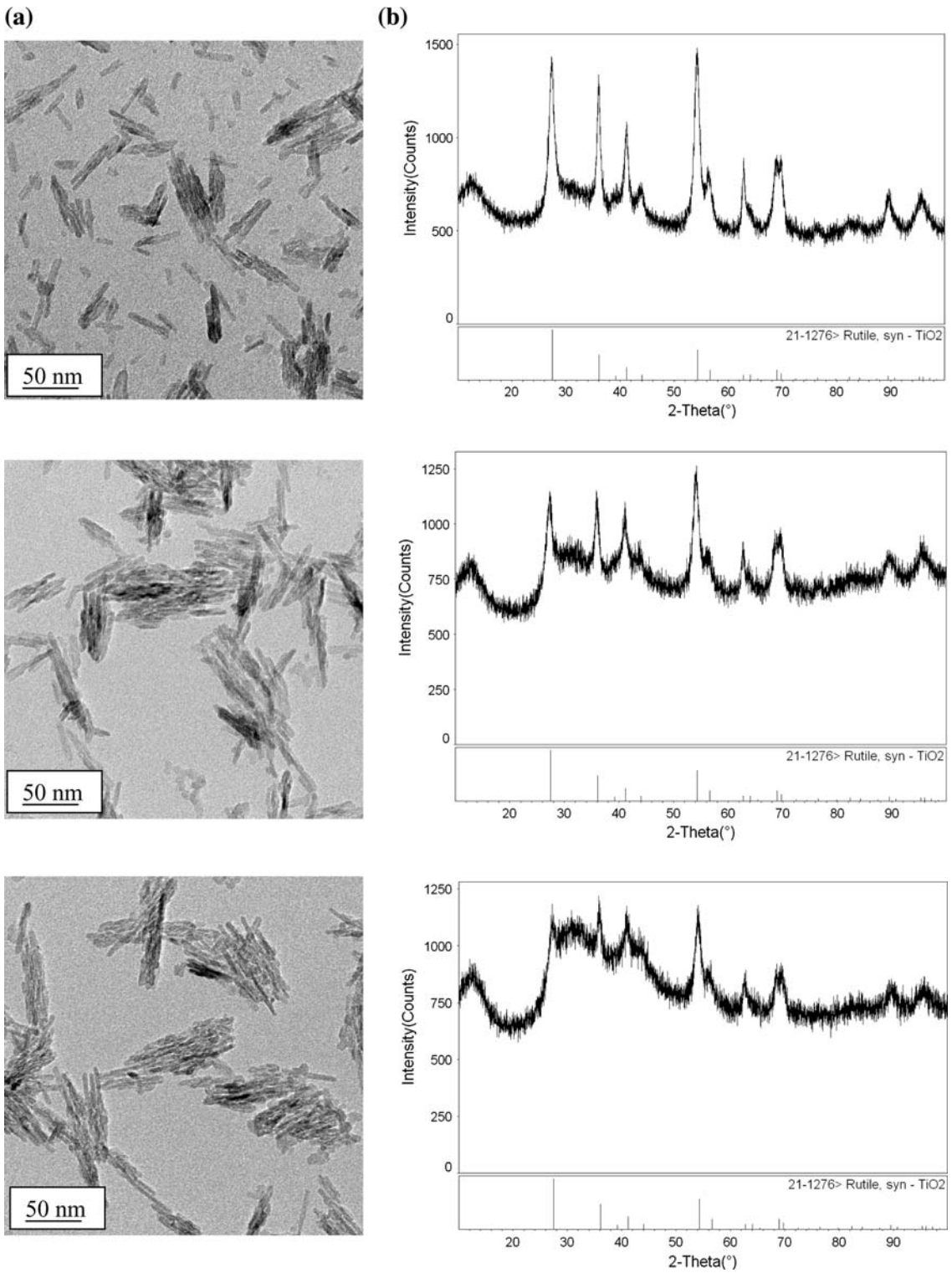

Fig. 12 TiO_2 materials generated from HX HYBR route using rutile starting nanomaterial: **a** TEM images with scale bars of: (i) 50 nm, (ii) 50 nm, and (iii) 10 nm and **b** PXRD pattern

morphologies, in comparison to the SOLVO route. For anatase, 30–40 nm nanosquares were observed for all acids; whereas, nanorods (aspect ratio of 10) were generated using rutile materials.

The development of the HYBR route will allow for large-scale processing of the morphologically varied nanowires (high pH) and nanosquares (low pH). Now that the effect that the starting nanoseeds have on the final

phase has been elucidated, further work to understand the growth processes and control over the final properties of these systems is underway.

Acknowledgements For support of this research, the authors thank the U.S. Department of Energy, Office of Basic Energy Science, Division of Material Sciences and Engineering and the Laboratory Directed Research and Development (LDRD) program at Sandia National Laboratories. Sandia is a multiprogram laboratory operated by Sandia Corporation, a Lockheed Martin Company, for the United States Department of Energy's National Nuclear Security Administration under Contract DE-AC04-94AL85000.

References

1. Kislyuk VV, Dimitriev OP (2008) J Nanosci Nanotech 8:131
2. Zhu BL, Li KO, Zhang SM, Wu SH, Huang WP (2008) Prog Chem 20:48
3. van de Krol R, Liang YQ, Schoonman J (2008) J Mater Chem 18:2311
4. Qui JJ, Yu WD, Gao XD, Li XM, He WZ, Park SJ, Kim HK, Hwang YH (2008) J Sol-Gel Sci Tech 47:187
5. Masuda Y, Kato K (2008) Cryst Growth Des 8:3213
6. Ban T, Nakatani T, Uehara Y, Ohya Y (2008) Cryst Growth Des 8:935
7. Bavyin DV, Cressey BA, Walsh FC (2007) Aust J Chem 60:95
8. Yuan ZY, Su BL (2004) Coll Surf A—Phys Engin Asp 241:173
9. Wang BX, Shi Y, Xue DF (2007) J Solid State Chem 180:1028
10. Khan SUM, Sultana T (2003) Solar Energy Mater Solar Cells 76:211
11. Hakuta Y, Hayashi H, Arai K (2004) Mater Res Soc Symp Proc 789:263
12. Dong W, Cogbill A, Zhang T, Ghosh S, Tian ZR (2006) J Phys Chem B Lett 110:16819
13. Tian ZR, Voigt JA, Liu J, McKenzie B, Xu H (2003) J Am Chem Soc 125:12384
14. Penn RL, Banfield JF (1999) Geochimica Cosmochim Acta 63:1549
15. Gao Y, Elder SA (2000) Mater Lett 44:228
16. Chemseddine A, Mortiz T (1999) Eur J Inorg Chem 2:235
17. Sugimoto T, Zhou X, Muramatsu A (2003) J Colloid Interface Sci 259:43
18. Finnegan MP, Zhang H, Banfield JF (2007) J Phys Chem C 111:1962
19. Li Y, White TJ, Lim SH (2004) J Solid State Chem 177:1372
20. Sugimoto T, Zhou X, Muramatsu A (2003) J Colloid Interface Sci 259:53
21. Zaban A, Aruna ST, Tirosh S, Gregg BA, Mastai Y (2000) J Phys Chem B 104:4130
22. Aruna ST, Tirosh S, Zaban A (2000) J Mater Chem 10:2388
23. Barnard AS, Curtiss LA (2005) NanoLetters 5:1261
24. Roy SC, Paulose M, Grimes CA (2007) Biomaterials 28:4667
25. Bright E, Readey DW (1987) J Am Ceram Soc 70:900
26. Schmuki P, Bauer S, Kleber S (2006) Electrochm Commun 8:1321
27. Wu G, Wang J, Thomas DF, Chen A (2008) Langmuir 24:3503
28. Lan Y, Gao XD, Zhu H, Zheng Z, Yan T, Wu F, Ringer SP, Song D (2005) Adv Funct Mater 15:1310
29. Chen XB, Mao SS (2006) J Nanosci Nanotech 6:906
30. Chen XB, Mao SS (2007) Chem Rev 107:2891
31. Tachikawa T, Fujitsuka M, Majima T (2007) J Phys Chem C 111:5259
32. Jwo CS, Tien DC, Teng TP, Chang H, Tsung TT, Liao CY, Lin CH (2005) Rev Adv Mater Sci 10:283
33. Tomovska R, Marinkovski M, Frajgar R (2007) NATO Sci Peace Security Series C-Envir Security 207
34. Swamy V (2008) Phys Rev B 77:195414
35. Sasaki T, Shimizu Y, Koshizaki N (2005) Rev Laser Engin 33:18
36. Theron J, Walker JA, Cloete TE (2008) Crit Rev Microbiol 34:43
37. Bogue RW (2004) Sensor Rev 24:253
38. Bruce PG, Scrosati B, M TJ (2008) Angew Chem IEEE 47:2930
39. Jing LQ, Qu YC, Wang BQ, Li SD, Jiang BJ, Yang LB, Fu W, Fu HG, Sun JZ (2006) Solar Energy Mater Solar Cells 90:1773
40. Hulteen JC, Martin CR (1997) J Mater Chem 7:1075
41. Ofir Y, Samanta B, Rotello VM (2008) Chem Soc Rev 37:1814
42. Balazs AC, Emrick T, Russell TP (2006) Science 314:1107
43. Vaia RA, Maguire JF (2007) Chem Mater 19:2736
44. Mackay ME, Tuteja A, Duxbury PM, Hwawker CJ, Van Horn B, Guan Z, Chen G, Krishnan RS (2006) Science 311:1740
45. Jade XRD Pattern Processing MDI, Inc., Livermore, CA (1999)
46. Daoud WA, Pang GKH (2006) J Phys Chem B 110:25746
47. Sugita M, Tsugi M, Abe M (1990) Bull Chem Soc Jpn 63:1978
48. Mer'kov AN, Bussen IV, Goiko EA, Kul'chitskaya EA, Men'shikov YP, Nedorezova AP (1973) Zap Vses Miner O-va 102:54
49. Valtchev V, Paillaud J-L, Mintova S, Kessler H (1999) Microporous Mesoporous Mater 32:287
50. Sandomirskii PA, Belov NV (1979) Sov Phys Crystallogr 24:686
51. Barnard AS, Xu H (2008) ACSNano 2:2237
52. Yeredla RR, Xu H (2008) Nanotechnology 19:1
53. Machesky ML, Wesolowski DJ, Fidley MK, Palmer DA, Rosenqvist J, Lvov SN, Fedkin M, Predota M, Vlcek L (2008) ECS Trans 11:151
54. Buchanan RC, Park T (1997) Materials crystal chemistry. Marcel Dekker, Inc., New York
55. Selloni A (2008) Nat Mater 7:613
56. Watanabe T, Nakajima A, Wang R, Minabe M, Koizumi S, Fujishima A, Hashimoto K (1999) Thin Solid Films 351:260